atmosphere

Article

Characteristics of Rainstorm Intensity and Its Future Risk Estimation in the Upstream of Yellow River Basin

Wanzhi Li [1,2], Ruishan Chen [2,3,*], Shao Sun [4], Di Yu [1], Min Wang [5], Caihong Liu [1] and Menziyi Qi [1]

[1] Qinghai Climate Center, Xining 810001, China
[2] Institute of Plateau Science and Sustainable Development, Xining 810001, China
[3] School of Design, Shanghai Jiaotong University, Shanghai 200030, China
[4] State Key Laboratory of Severe Weather (LASW), Chinese Academy of Meteorological Sciences, Beijing 100081, China
[5] Huangnan Prefecture Meteorological Bureau, Tongren 811300, China
* Correspondence: rschen@sjtu.edu.cn

Abstract: Under the background of climate warming, the occurrence of extreme events upstream of the Yellow River Basin has increased significantly. Extreme precipitation tends to be even more intense, and occurs more frequently. The impacts of various extreme weather and climate events in the basin have become increasingly complex, which is increasingly difficult to cope with and affects the basin's long-term stability and ecological security. Based on the daily precipitation data of 33 meteorological stations in the upper reaches of the Yellow River Basin from 1961 to 2021, this paper analyzes the characteristics of rainstorm intensity. Moreover, combined with the simulation results of 10 global climate models of the Coupled Model Intercomparison Project (CMIP6) and the social and economic prediction data from SSPs, it analyzes the possible changes of rainstorm disaster risk in the upper reaches of the Yellow River Basin in the 21st century, under the three emission scenarios of SSP126, SSP245, and SSP370. The results show that the precipitation in the upstream area of the Yellow River Basin is increasing at a rate of 8.1 mm per 10 years, and the number of rainstorm processes and their indicators is increasing, which indicates an increase in the extremeness of precipitation; the rainstorm process intensity index shows an increasing trend, especially in the northeast region with a concentrated population and economy, where the rainstorm process intensity index is high; it is estimated that the number of rainstorm days in low-, medium-, and high-risk scenarios will increase, which leads to an increase in the social risk by at least 60% by around 2050 (2036–2065); with the increasing disaster risk, the population exposure to rainstorm disasters is also on the rise. If no measures are taken, the population exposure will increase to 7.316 million people per day by around 2050, increasing by more than double, especially in the northeast. This study shows that, with the increasing rainstorm disaster risk and population exposure in the upper reaches of the Yellow River Basin, relevant measures need to be taken to ensure the safety of people's lives and property.

Keywords: rainstorm process; rainstorm intensity; risk estimation and mapping; CMIP6; risk prediction

check for updates

Citation: Li, W.; Chen, R.; Sun, S.; Yu, D.; Wang, M.; Liu, C.; Qi, M. Characteristics of Rainstorm Intensity and Its Future Risk Estimation in the Upstream of Yellow River Basin. *Atmosphere* **2022**, *13*, 2082. https://doi.org/10.3390/atmos13122082

Academic Editor: Haibo Liu

Received: 5 November 2022
Accepted: 8 December 2022
Published: 10 December 2022

1. Introduction

Under the background of climate warming, the frequency, intensity, and duration of extreme climate events are increasing, which will magnify and exacerbate the risk of future climate disasters [1–3] and have huge impacts on human life, agricultural production, and the social economy, etc. [4,5]. According to statistics, in the past 30 years, 86% of the world's major natural disasters, 59% of deaths, 84% of economic losses, and 91% of insurance losses were caused by meteorological and derived disasters. China has become one of the world's most seriously affected countries by meteorological disasters [6], where the disasters account for more than 70% of natural disasters in recent years [7]. It is estimated that the possibility of flooding, high temperatures, and other disaster risks in China in the future will also be further increased [8]. On the regional and global scales, precipitation changes are more localized than temperature changes. Therefore, extreme precipitation usually shows high regional complexity and spatial-temporal variation [9]. Local heavy rainfall is more likely to lead to severe meteorological disasters. For example, the "7.21" torrential rain in Beijing in 2012 [10], the extremely heavy rain in North China from 19 to 20 July in 2016 [11], the extremely heavy rain in Hubei Province from 18 to 20 July in 2016 [12], the "5.7" extremely heavy rain in Guangzhou in 2017 [13], and the "7.20" extremely heavy rain in Zhengzhou in 2021 [14] all caused severe floods and their derivative disasters, high casualties, and economic and property losses. Therefore, analyzing the characteristics of rainstorm disasters and predicting their future risks is very meaningful.

Human-induced global warming has increased the frequency, intensity and number of heavy precipitation events worldwide. As the atmosphere warms, it contains more moisture, which means more rain during storms [15,16]. Climate change research advances have helped improve predictions of hydrologic extremes, with potentially severe implications for human societies and natural landscapes. The impact of precipitation is mainly reflected by the overall changes in the precipitation amount, intensity, spatial and temporal distribution, and the increase in extreme precipitation events, the most direct impact of which is the change in the intensity of precipitation erosion forces and the occurrence of extreme precipitation due to the changes in precipitation [17–20]. At the same time, the increased uncertainty of extreme precipitation and the influence of human activities lead to certain types of extreme precipitation patterns that can cause significant stress on river hydrology, and thus increase the risk of regional flood control [21,22].

In the rainstorm hazard census, the intensity of the rainstorm process is usually calculated to assess the risk level of the rainstorm process. Scholars have conducted related studies. Wang et al. established a comprehensive intensity assessment model and classification criteria for precipitation processes in four rainstorm-hazard-sensitive areas in China using three indicators: rainfall intensity, coverage area, and duration [23]. Zou et al. selected four indicators of maximum daily rainfall, maximum process rainfall, and rainstorm extent and duration, and constructed a comprehensive intensity assessment model of the regional rainstorm process and the comprehensive intensity classification criteria in Fujian Province [24]. Han et al. established a comprehensive rainstorm disaster assessment index for Liaoning Province, based on the average amount of rainfall, rainfall intensity extremes, and coverage size [25]. Moderate rain, heavy rain, and rainstorm events are estimated to increase significantly nationwide at the end of the 21st century [26]. The population exposure to extreme precipitation in China is also expected to increase by nearly 22% [27], aggravating the potential risk of disasters caused by rainstorms [28–31]. Adequate measures need to be taken in advance [32].

Existing studies have analyzed the runoff characteristics, precipitation characteristics, and their causes of formation in the Yellow River Basin [33–35]. However, few have concentrated on the characteristics of rainstorm intensity in the basin and the direction of future risk estimation. Currently, the Coupled Model Intercomparison Project is at a sixth stage (CMIP6), and has improved resolution, physical processes, and parameterization [36]. Moreover, compared with CMIP5, CMIP6 can enable the simulation results to be closer to the observations [37,38]. Based on CMIP6, studies have simulated and predicted the future temperature in the upper reaches of the Yellow River. This paper aims to solve the following key questions, by analyzing the characteristics of rainstorm intensity and estimating the future risk in the upper reaches of the Yellow River Basin: (1) Are the extremes of precipitation in the upper reaches of the Yellow River Basin increasing? How about their distribution? (2) Under the background of climate change, what about the future rainstorm disaster risk in the upper reaches of the Yellow River Basin? Where is the highest risk?

2. Data and Methods

2.1. Study Area

Qinghai Province is located in northwestern China, between latitude 31°36′–39°19′ north and longitude 89°35′–103°04′ east, as the headstream and mainstream area of the Yellow River; it has a drainage area of 152,300 km^2 (accounting for 21% of the Yellow River Basin), a drainage length of 1983 km (taking up 31% of the Yellow River), and the annual runoff out of the province accounts for 49.2% of the total flow of the Yellow River [39]. It impacts the sustainable development and utilization of water resources in the Yellow River Basin. The upper reaches of the Yellow River Basin are the population and economic agglomeration area of Qinghai Province, as well as the high precipitation and rainstorm-disaster-prone areas. For example, the flash flood disaster in Datong on 18 August 2022 caused heavy casualties and economic and property losses. Extreme rainstorms and the complex geographical environment are the main reasons for the frequent occurrence of rainstorm disasters in the upper reaches of the Yellow River Basin.

The upstream area of the Yellow River Basin is the source and mainstream area of the Yellow River, and the part of its watershed overlapping with the administrative region of Qinghai Province is located in the eastern part of Qinghai Province (Figure 1). The area of this region is 277,800 km^2, with a total population of 5,252,100, and a GDP of 226.44 billion CNY as of the end of 2019, accounting for 39.9%, 86.4%, and 76.3% of the province, respectively. The region is a significant ecological security barrier and a core area for high-quality development. The environmental quality in the study area significantly impacts the Sanjiangyuan Basin's ecological functions, the north and south slopes of the Qilian Mountains, and the arid eastern mountains. The upper reaches of the Yellow River Basin belong to the highland continental climate, with a low temperature and low precipitation. The annual average temperature is −3.8~9.5°C, which is high in the east and low in the south and north; annual precipitation is 256.7~742.0 mm, with more in the south and less in the north; annual rainstorm days last 9~69 days, with a greater number in the north and lower in the south. The distribution of rainstorm days is similar to the distribution of the annual average temperature, which is different from the distribution of the annual precipitation.

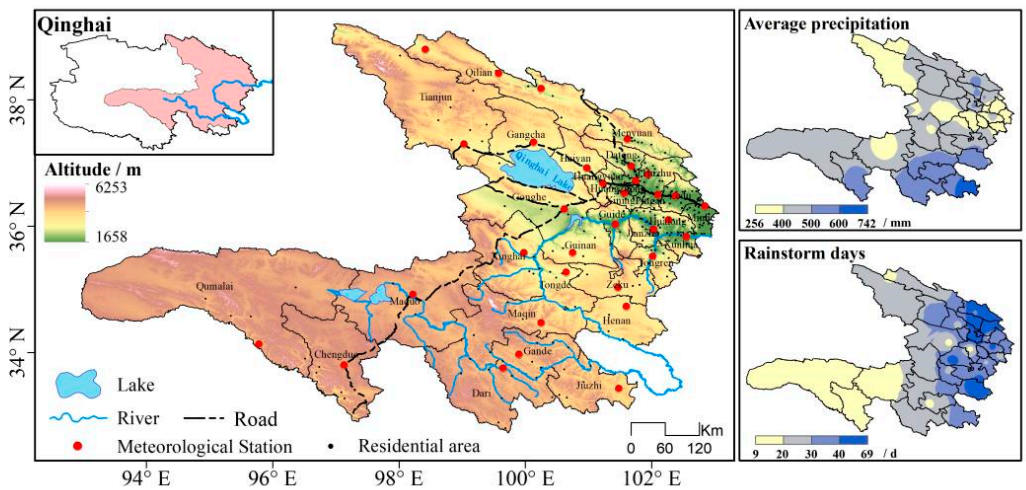

Figure 1. Map of the location of the upper Yellow River Basin.

2.2. Data Sources

The meteorological data were obtained from the Qinghai Meteorological Information Center, including the daily precipitation observations from 33 national meteorological observation stations (including national benchmark stations, basic stations, and general stations). The time that the meteorological data was obtained was selected from 1961 to 2021, and all data were subjected to strict quality control (Figure 2). The mean values in the paper are adopted from the standard climatic mean (mean values for 1991–2020).

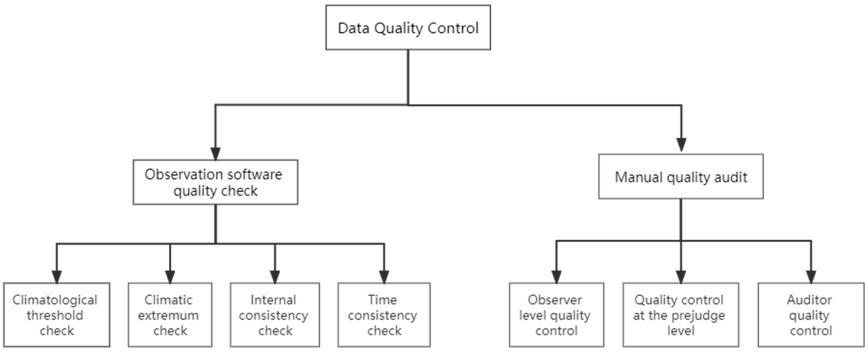

Figure 2. Data quality control flow chart.

The simulations from 10 climate models in the CMIP6 project were selected through the availability of daily precipitation for the historical run and future scenario runs (i.e., SSP1-2.6, SSP2-4.5, and SSP5-8.5) [40]. The multimodal ensemble mean (MME) method can effectively reduce the uncertainty of the simulations and presents the spatial pattern of precipitation extremes, which has been verified in numerous studies [41,42]. Only the first simulation member (r1i1p1f1) of each model is adopted. We resample all outputs of the 10 models to a common 0.25×0.25 resolution by using bilinear interpolation and only the data in the upper reaches of the Yellow River Basin.

Shared Socioeconomic Pathways (SSPs) are coupled with representative concentration pathways (RCPs), often applied to future project scenarios of socioeconomic development [43]. The projected population datasets are available at Socioeconomic Data and Applications Center (SEDAC), with ten-year intervals of 2010–2100 and a precision of 1 km on global land [44]. SSP1, SSP2, and SSP5 scenarios were selected to present population changes corresponding to low-, moderate-, and high-emission scenarios (i.e., RCP2.6, RCP4.5, and RCP8.5), respectively.

2.3. Methods

Since the rainfall in Qinghai province is small, the standard of rainstorm disaster is reached when the daily rainfall reaches $\geq$25 mm [45]. Therefore, in this paper, the rainfall process with $\geq$10 mm rainfall at a single station lasting $\geq$1 day and reaching $\geq$25 mm rainfall occurring during the process is called the rainstorm process.

The weighted comprehensive evaluation method is used to calculate the intensity of the rainstorm process [46]. It integrates the degree of influence of each indicator on the overall object. The effects of each specific indicator are combined and a quantitative indicator is used to focus on the degree of influence of the overall evaluation object. The calculation process begins with the normalization of each evaluation indicator [47]. Normalization is transforming a quantified value into a dimensionless value, which eliminates the quantified differences of each indicator. The calculation formula is:

$$X_{ij} = \frac{R_{ij} - R_{imin}}{R_{imax} - R_{imin}}, \tag{1}$$

where X_{ij} is the normalized value of the ith indicator at site j; R_{ij} is the ith indicator value at site j; R_{imin} and R_{imax} are the minimum and maximum values of the ith indicator value, respectively.

In this study, the maximum daily rainfall of the rainstorm process, the accumulated rainfall of the process, and the duration of the process are selected as the index factors for calculating the intensity of the rainstorm process. The intensity index of the rainstorm process is obtained by weighted summation. The calculation formula is:

$$\mathrm{IR} = \mathrm{A} \times \mathrm{R}_{24\mathrm{pre}} + \mathrm{B} \times \mathrm{R}_{\mathrm{pre}} + \mathrm{C} \times \mathrm{R}_{\mathrm{day}}, \tag{2}$$

where IR is the intensity index of the rainstorm process, R_{24pre} is the process daily maximum rainfall, R_{pre} is the process cumulative rainfall, and R_{day} is the process duration days. A, B, and C are the weight coefficients of each index, which are determined by the information entropy assignment method. This method is based on the actual data of each sample used to find the optimal weights, avoiding artificial influencing factors; therefore, the index weights given are more objective and thus have higher reproducibility and credibility. The specific calculation method is described in reference [48].

A linear trend equation, a significance t-test [49], and the Yue–Pilon [50] method were used in performing the statistical analysis. The linear trend equation is:

$$x_i = a + b \times t_i. \tag{3}$$

The climate variable of a sample size is denoted by x_i, the corresponding event is denoted by t_i, a univariate linear regression is created between x_i and $t_{i,}$ a is the regression constant, and b is the regression coefficient.

3. Characteristics of the Intensity Change of the Rainstorm Process

3.1. Precipitation Variation Characteristics

From 1961 to 2021, the annual average precipitation upstream of the Yellow River Basin was 330.5 mm, with an overall increase of 8.1 mm/10a(years abbreviated as a). In terms of chronological changes, the annual precipitation fluctuated greatly in the early 1960s, and did not change significantly from the late 1960s to the 1990s. Moreover, the 1990s was the period with the lowest annual precipitation, which was only 308.8 mm. At the beginning of the 21st century, the annual precipitation began to increase significantly. Since the 2010s, it has been the period with the highest annual precipitation, reaching 346.2 mm. The year with the highest annual precipitation was 2018, which reached 429.4 mm (Figure 3a). From the perspective of spatial distribution, the annual precipitation in Minhe, Henan, and Huzhu, showed a decreasing trend, while the annual precipitation in the rest of the regions mainly increased, with an increase of 2.3~22.1 mm/10a. Additionally, the middle Yellow River Basin is the region with the most significant annual precipitation increase, with Guinan having the most significant increase, reaching 22.1 mm/10a (Figure 3b).

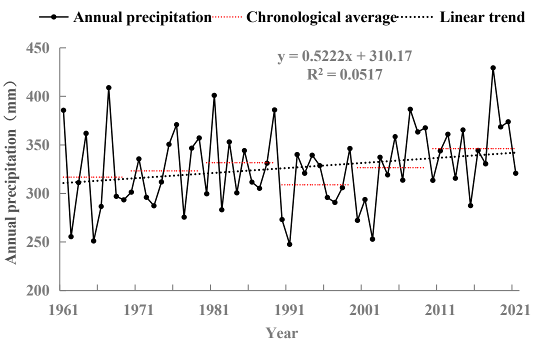

(**a**)

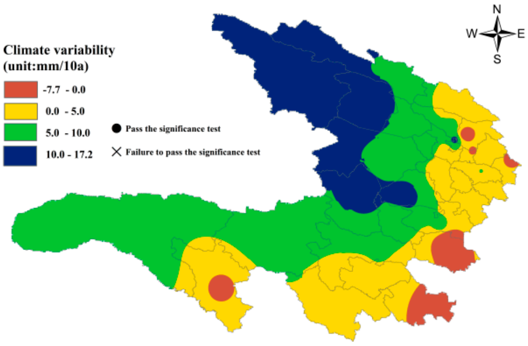

(**b**)

Figure 3. Variation curve (**a**) and spatial distribution of variability (**b**) of annual precipitation in the upstream of Yellow River Basin from 1961 to 2021.

3.2. Index Characteristics of the Rainstorm Process

From 1961 to 2021, the annual average number of a rainstorm upstream of the Yellow River Basin was 35.5 stations, showing an overall increasing trend, with an increase of 2.3 stations/10a. The number of rainstorms was relatively few from the 1960s to the 1980s, and began to increase in the 1990s. The period of the 2010s had the heaviest precipitation processes, with an average of 39.2 stations per year, of which the highest frequency was in 2018, with 77 stations (Figure 4a).

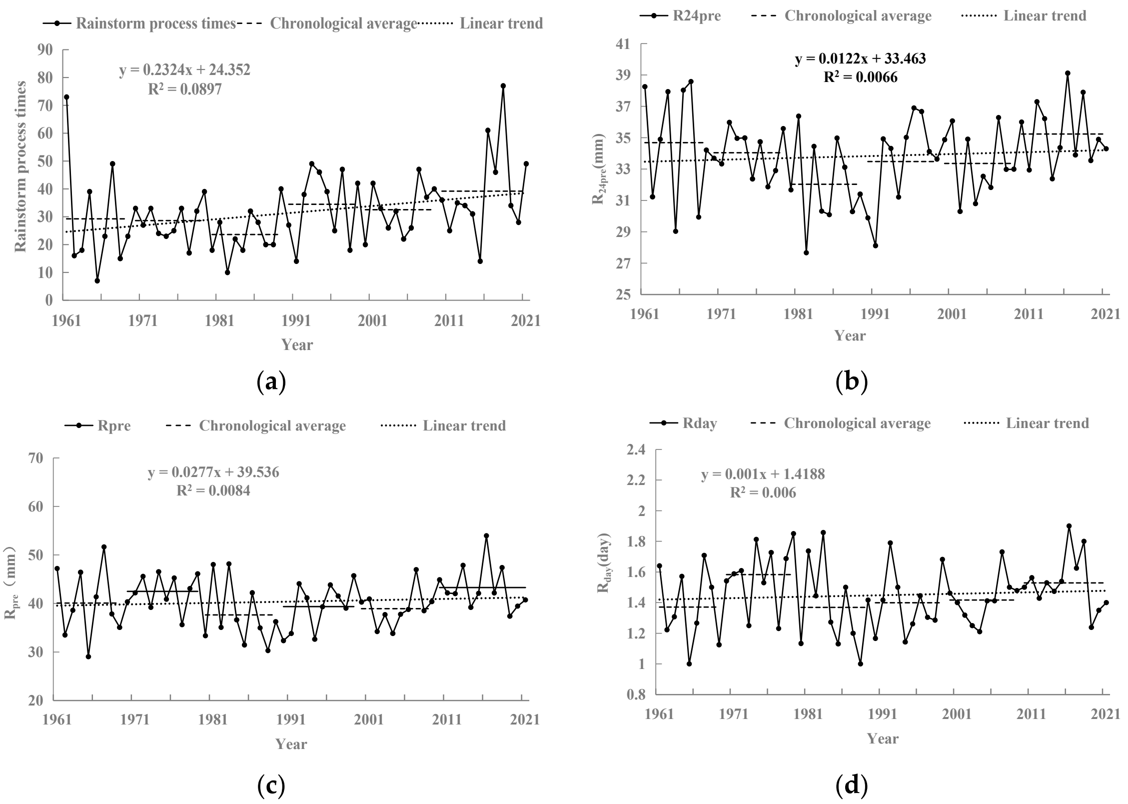

Figure 4. Variation curves of the number of rainstorm processes (**a**), maximum daily precipitation (**b**), accumulated precipitation (**c**), and duration of precipitation (**d**) in the upstream of Yellow River Basin from 1961 to 2021.

During the rainstorm, the average daily maximum precipitation, cumulative precipitation, and duration of precipitation were 34.4 mm, 64.7 mm, and 2 days, respectively, therefore all show an increasing trend. The maximum daily precipitation showed a trend of first decreasing and then increasing, with a minimum in the 1980s, and it continued to increase, reaching a maximum in the 1910s (Figure 4b). The accumulated precipitation fluctuated, and the minimum and maximum values also appeared in the 1980s and after the 21st century (Figure 4c), respectively. Except for the high value in the 1970s, the duration of precipitation showed a steady upward trend in other years (Figure 4d). Judging from the changes of various indices, not only the number of rainstorm processes in the upstream of Yellow River Basin increased, but also the various indices of the rainstorm processes showed an increasing trend, indicating that the extremeness of precipitation was also increasing.

From the perspective of spatial distribution, rainstorms tended to occur more in the east and less in the west. The number of rainstorms in Xining, Huangzhong, Datong, and Huzhu in the northeastern basin, and Henan in the southeast are all over 50. Huangzhong had the most frequent precipitation events, reaching a total of 69 times, which occurred more than 2 times a year on average (Figure 5a). The distribution trend of the average daily maximum precipitation during the rainfall process is generally consistent with the distribution trend of the number of rainfall processes. The high-value areas are mainly distributed in Datong, Xining, Minhe, Huzhu, and Huang in the northeast of the Yellow River Basin. In the high-value area, Datong had the largest average daily precipitation, with a value of 41.3 mm (Figure 5b). The distribution characteristics of the accumulated precipitation and the duration of the precipitation process are essentially the same, and the overall distribution trend is high in the north and south and low in the middle areas. Among them, the high-value areas of accumulated precipitation include Gangcha, Datong, Menyuan, Tianjun, and Huzhu, and the accumulated precipitation is above 45 mm. Furthermore, there are two high-value areas in the southeast, Henan and Jiuzhi (Figure 5c). The duration of the rainstorm process lasts longer in the high-value southern regions, including in Jiuzhi, Qingshuihe, Maqin, Qumalai, Dari, Henan, Zeku, and Guinan, among other places. The northern high-value areas include Datong, Qilian, Menyuan, Gangcha, Haiyan, and Tianjun, and the average duration of precipitation is more than 1.5 days (Figure 5d). Henan County is the region with the largest average accumulated precipitation and the longest duration of precipitation, with values of 52.5 mm and 2 d, respectively. The maximum historical daily precipitation was 119.9 mm in Datong in 2013, the maximum accumulated precipitation was 154.3 mm in Henan County in 2016, and the maximum duration of the process was 6 days in Jiuzhi in 1979.

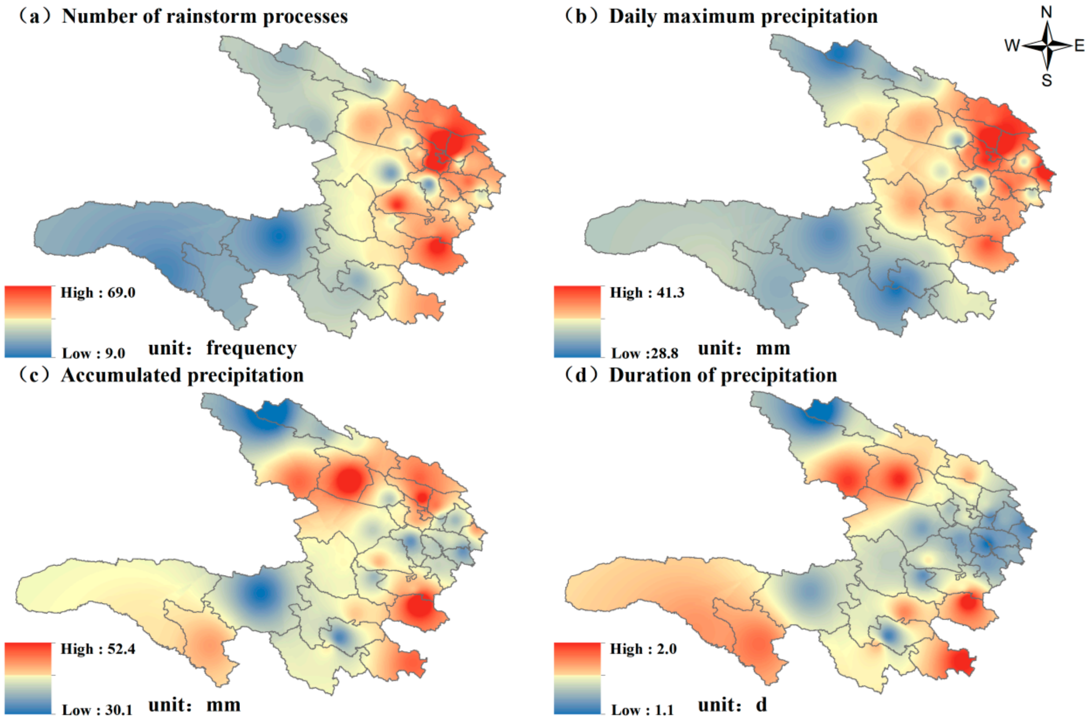

Figure 5. Spatial distribution of the number of heavy precipitation processes (**a**), daily maximum precipitation (**b**), accumulated precipitation (**c**), and duration of precipitation (**d**) in the upstream of Yellow River Basin from 1961 to 2021.

3.3. Intensity Characteristics of the Rainstorm Process

The intensity index of the rainstorm process is calculated according to Formula (2), and the larger the value, the higher the possibility of causing disasters. From 1961 to 2021, the intensity index of the rainstorm process upstream of the Yellow River Basin showed an overall increasing trend. From the perspective of chronological changes, it began to increase slowly after experiencing the high-value stage of the rainstorm process intensity index in the 1970s. The increasing trend after the 21st century is the most obvious, and it is the period with the highest intensity of the rainstorm process. In terms of years, 2018 was the year with the largest rainstorm process intensity index (Figure 6a). In terms of spatial distribution, there are two high-value centers of the rainstorm process intensity index in the northern and southern parts of the Yellow River Basin. Among them, the high-value and middle-value areas in the north include eight areas: Datong, Gangcha, Huzhu, Menyuan, Xining, Huangzhong, Tianjun, and Minhe. The high-value centers in the south include Henan and Jiuzhi. The rainstorm process intensity index was low in the northwestern Yellow River Basin and most areas of the source of the Yellow River (Figure 6b). From the spatial distribution of the intensity index of the rainstorm process, it can be seen that most of the administrative regions where the high-value areas are located are the areas with the most concentrated economy and population in Qinghai Province, which makes the region more vulnerable to rainstorm disasters.

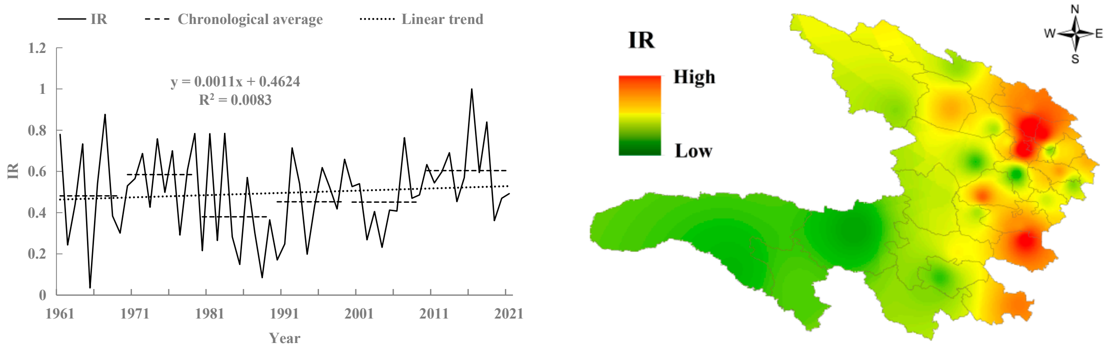

(**a**) (**b**)

Figure 6. Changes in the risk level of rainstorm disasters under different climatic conditions in the upstream of the Yellow River Basin. (**a**) overall trend (**b**) spatial distribution.

4. Future Climate Risk Estimation for Rainstorm Disasters

4.1. Estimated Number of Days of Rainstorms in Future Scenarios

The number of days of a rainstorm upstream of the Yellow River Basin during the base period (1991–2020) is 1.1 d. The model estimation indicates that the frequency of rainstorms upstream of Yellow River Basin increases significantly in future scenarios, leading to increasing levels of combined climate risk. Even with the most stringent of carbon reduction measures in the future (the SSP126 scenario), the number of rainstorm days in the upstream of Yellow River Basin is expected to rise to 1.5 d by around 2050 (2036–2065), leading to a 60% increase in the socioeconomic risk index. In the medium-emission scenario (SSP245), the number of rainstorm days will rise to 1.6 days in around 2050, leading to a 67% increase in the socioeconomic risk index. If fossil fuels continue to be used as the main energy source (the SSP370 scenario), the number of rainstorm days in the upstream of Yellow River Basin will rise to 1.8 days in around 2050, leading to a doubling of the socioeconomic risk index from the historical base period (Figure omitted).

In terms of administrative districts, Xining, Datong, Huangzhong, Huzhu, and Henan County have the highest number of rainstorm days, and the historical base period (1991–2020) has reached more than 1.5 days per year. Under the future low- and medium-emission scenarios, it is expected to rise to more than 2.4 days around 2050, which is the most dramatic response to climate warming within the upstream Yellow River Basin (Figure 7a,b). Under the high-emission scenario, the number of days of rainstorm in Huangzhong is expected to exceed 3 days (Figure 7c,d).

4.2. Population Exposure Risk Estimation for Future Scenarios

The overlay of the predicted results by the number of rainstorm days and population shows that the population exposure in upstream of the Yellow River Basin during the historical base period is 3.833 million people per day (mpd), among which, Datong, Huzhu, and Huangzhong have the highest population exposure with 0.652 mpd, 0.574 mpd and 0.526 mpd. Under the low-emission scenario, it is expected that the population exposure to rainstorm hazards in the upstream of the Yellow River Basin will rise to 5.613 mpd around 2050, which is an increase of 46%, with Datong, Huzhu, and Xining all reaching over 0.526 mpd (Figure 8a). Under the medium-emission scenario, the population exposure to rainstorm hazards in the source of the Yellow River is expected to rise to 6.036 mpd around 2050, and the three county-level units with the highest exposure are expected to be Xining (0.956 mpd), Datong (0.919 mpd), and Huzhu (0.871 mpd) (Figure 8b). If no emission reduction measures are taken and the current carbon emission intensity continues, the population exposure will rise to 7.316 mpd around 2050, among which, the population exposure of rainstorm disasters in the Datong, Xining, and Huzhu counties (districts) will exceed one million people per day (Figure 8c). In particular, the population exposure of the rainstorm disaster in Datong will increase by 0.314 mpd; compared with the low-emission scenario, the values for Huzhu and Huangzhong both increase by more than 0.2 mpd (Figure 8d).

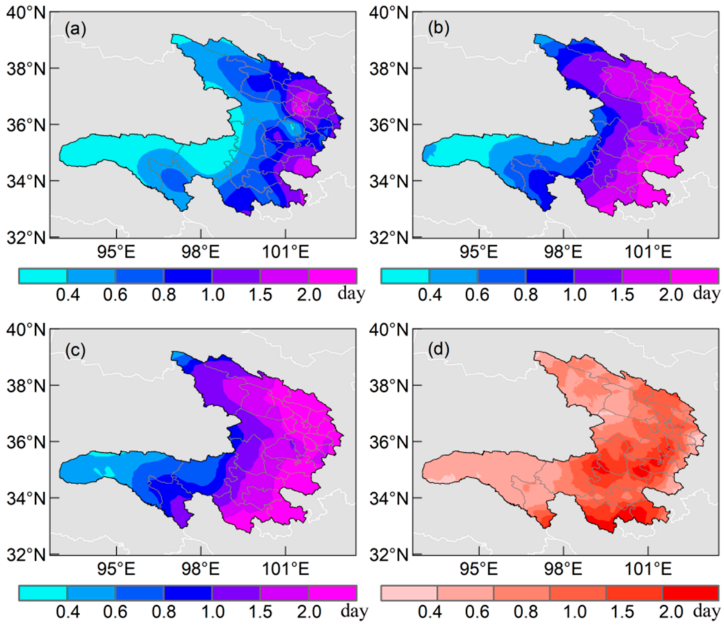

Figure 7. Spatial distribution of rainstorm days around 2050 (2036–2065) in the upstream of Yellow River Basin in future scenarios: (**a**) low-emission scenario SSP126, (**b**) medium-emission scenario SSP245, (**c**) high-emission scenario SSP370, (**d**) the difference in rainstorm days between high- and low-emission scenarios.

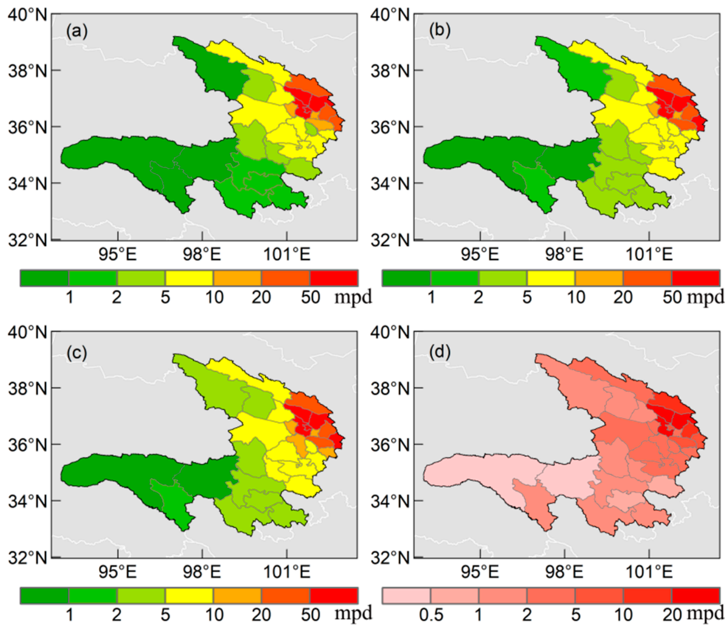

Figure 8. Spatial distribution of population exposure to rainstorm disasters upstream of the Yellow River Basin at around 2050 (2036–2065) in future scenarios: (**a**) low-discharge scenario SSP126, (**b**) medium-discharge scenario sSSP245, (**c**) high-discharge scenario SSP370, (**d**) difference in population exposure between high- and low-discharge scenarios.

5. Discussion and Conclusions

This study analyzed the rainstorm intensity characteristics based on the daily rainfall data of 33 meteorological stations upstream of the Yellow River Basin from 1961 to 2021. The simulation results of 10 global climate models of CMIP6 and the socioeconomic prediction data of SSPs were used to analyze the possible changes of rainstorm hazard risk in the upstream of the Yellow River Basin region in the 21st century in three emission scenarios (SSP126, SSP245, and SSP370). The conclusions are as follows:

1. From 1961 to 2021, rainfall upstream of the Yellow River Basin showed an overall increasing trend, with an increased rate of 8.1 mm/10a. In the 21st century, the rising annual rainfall trend is becoming particularly significant. The maximum daily rainfall, accumulated rainfall, and the number of days of duration during rainstorms all show a rising trend, and the extremity of rainfall increases;
2. From 1961 to 2021, the intensity index of the rainstorm process showed an increasing trend. The increase has become pronounced since the beginning of the 21st century, which is the period with the highest value of the intensity index of the rainstorm process. Most of the administrative districts where the high-value areas are located are the most economically and population-concentrated areas in Qinghai Province. The risk of rainstorm disasters and possible damages will also increase;
3. The low-, medium-, and high- emission scenarios are all expected to show an increasing trend in the number of rainstorm days by around 2050 (2036–2065). Among them, the low-emission scenario will lead to at least a 60% increase in social risk. The medium-emission scenario will lead to a 67% increase in the socioeconomic risk index. In contrast, the high-emission scenario will lead to a doubling of the socioeconomic risk index from the historical base period.
4. As the hazards increase, the population exposure to the rainstorm hazards will also rise. If no measures are taken, the population exposure will rise to 7.316 million per day around 2050. This has more than doubled compared to the base period, with the increase being particularly significant in the northeast.

In the background of global warming, rainfall upstream of the Yellow River Basin is increasing. At the same time, the extremes of precipitation are increasing. The increasing trend is particularly evident in the northeastern basin areas where the population and economy are more concentrated, further increasing the risk of rainstorm disasters. The CMIP6 model's prediction of the future rainstorm hazard risk in the watershed suggests that the social risk due to rainstorm hazards will increase under all three future low-, medium-, and high-emission scenarios, with even the low-emission scenario leading to a 60% increase in risk. The population's exposure to rainstorm hazards will also tend to increase, and the significant area of increase will also be in the northeastern part of the basin. The risk situation for future rainstorm events in the region is critical. There is an urgent need to incorporate climate adaptation strategies into future urban development to better respond to the climate risks associated with extreme rainfall events. The results from this research are consistent with the research results of Su and Sun et al. [51,52]. At the same time, the increased risk of rainstorm hazards may pose new challenges to economic sustainability. It may increase urban-rural migration and thus affect the geospatial distribution of social exposure, which needs to be considered in local climate risk management. In future urban construction, we can take different defensive measures according to the pattern and impact of rainstorm disasters, such as improving urban flood control and drainage standards, building sponge cities, raising public awareness, increasing extreme rainstorm warnings, and purchasing urban flood insurance, in order to better cope with the climate risks associated with extreme rainstorm events.

In this paper, the storm process and its indicators were analyzed, and its intensity was calculated. However, in this study, only meteorological elements were considered in analyzing the impact of heavy rainfall in the upper reaches of the Yellow River, and the considerations of topography, water systems, and other disaster-generating environments were missing. In addition, the 33 meteorological observation stations are relatively few compared to the extent of the upper Yellow River area, and do not provide a good characterization of the spatial distribution. In future studies, additional data could be introduced to create a composite index that describes the multidimensional characteristics of climate extremes (e.g., the peak intensity and duration).

Author Contributions: Conceptualization, W.L. and R.C.; validation, W.L., D.Y. and M.Q.; formal analysis, W.L. and S.S.; data curation, M.W. and C.L.; writing—original draft preparation, W.L. and R.C.; writing—review and editing, W.L.; visualization, D.Y. and S.S.; funding acquisition, W.L. All authors have read and agreed to the published version of the manuscript.

Funding: This study was jointly funded by the Second Integrated Scientific Expedition on Qinghai-Tibet Plateau (NO. 2019QZKK0906), the Key Soft Science Project of China Meteorological Administration (NO. 2022DIANXM13), the National Natural Science Foundation of China (NO. 42065003), and the Qinghai Provincial Science and Technology Department (NO. 2021-ZJ-757).

Institutional Review Board Statement: Not applicable.

Informed Consent Statement: Not applicable.

Data Availability Statement: No new data were created or analyzed in this study. Data sharing is not applicable to this article.

Acknowledgments: We acknowledge support from the above funding projects. Acknowledgments also to the Applications Center (SEDAC) for providing the population projections based on the Shared Socioeconomic Pathways (https://sedac.ciesin.columbia.edu/data/set/popdynamics-1-km-downscaledpop-base-year-projection-ssp-2000-2100-rev01. Accessed on 6 May 2022).

Conflicts of Interest: The authors declare no conflict of interest.

References

1. Diffenbaugh, N.S.; Singh, D.; Mankin, J.S.; Horton, D.E.; Swain, D.L.; Touma, D.; Charland, A.; Liu, Y.; Haugen, M.; Tsiang, M.; et al. Quantifying the influence of global warming on unprecedented extreme climate events. *Proc. Natl. Acad. Sci. USA* **2017**, *114*, 4881–4886. [CrossRef] [PubMed]
2. Coumou, D.; Rahmstorf, S. A decade of weather extremes. *Nat. Clim. Change* **2012**, *2*, 491–496. [CrossRef]
3. Toreti, A.; Naveau, P.; Zampieri, M.; Schindler, A.; Scoccimarro, E.; Xoplaki, E.; Dijkstra, H.A.; Gualdi, S.; Luterbacher, J. Projections of global changes in precipitation extremes from coupled model intercomparison project phase 5 models. *Geophys. Res. Lett.* **2013**, *40*, 4887–4892. [CrossRef]
4. Lipczynska-Kochany, E. Effect of climate change on humic substances and associated impacts on the quality of surface water and groundwater: A review. *Sci Total Environ.* **2018**, *640–641*, 1548–1565. [CrossRef] [PubMed]
5. Jiang, T.; Su, B.; Huang, J.; Zhai, J.; Kundzewicz, Z.W. Each 0.5 °C of warming increases annual flood losses in china by more than US$60 Billion. *Bull. Am. Meteorol. Soc.* **2020**, *101*, E1464–E1474. [CrossRef]
6. Cai, T.; Li, X.; Ding, X.; Wang, J.; Zhan, J. Flood risk assessment based on hydrodynamic model and fuzzy comprehensive evaluation with GIS technique. *Int. Disaster Risk Reduct.* **2019**, *35*, 101077. [CrossRef]
7. Wang, G.; Li, X.; Wu, X.; Yu, J. The rainstorm comprehensive economic loss assessment based on CGE model: Using a July heavy rainstorm in Beijing as an example. *Nat. Hazards.* **2015**, *76*, 839–854. [CrossRef]
8. Xu, Y.; Zhang, B.; Zhou, B.T.; Dong, S.Y.; Yu, L.; Li, R.K. Projected risk of flooding disaster in China based on CMIP5 models. *Clim. Change Res.* **2014**, *10*, 268–275. [CrossRef]
9. Xu, L.; Wang, A.; Wang, D.; Wang, H. Hot spots of climate extremes in the future. *J. Geophys. Res. Atmos.* **2019**, *124*, 3035–3049. [CrossRef]
10. Chen, Y.; Sun, J.; Xu, J.; Yang, S.; Sheng, J. Analysis and thinking on the extremes of the 21 July 2012 torrential rain in Beijing part I: Observation and thinking. *Meteor. Mon.* **2012**, *38*, 1255–1266. [CrossRef]
11. Fu, J.L.; Ma, X.K.; Chen, T.; Zhang, F.; Zhang, X.D.; Sun, J.; Quan, W.Q.; Yang, S.N.; Shen, X.L. Characteristics and synoptic mechanism of the July 2016 extreme precipitation event in North China. *Meteor. Mon.* **2017**, *43*, 528–539. [CrossRef]
12. Zhao, X.T.; Wang, X.f.; Wang, J.; Wang, X.K.; Xiao, Y.J.; Leng, L.; Fu, Z.K. Analysis of mesoscale characteristics of torrential rainfall in Hubei Province during 18–20 July 2016. *Meteor. Mon.* **2020**, *46*, 490–502. [CrossRef]
13. Xu, G.Q.; Zhao, C.Y. Impact of background field in the numerical simulation of extremely severe rainstorm in Guangzhou on 7 May 2017. *J. Meteor. Mon.* **2019**, *45*, 1642–1650. [CrossRef]
14. Wang, Z.Y.; Yao, C.; Dong, J.L.; Yang, H. Precipitation characteristic and urban flooding influence of "7·20" extreme rainstorm in Zhengzhou. *J. Hohai Univ.* **2022**, *50*, 17–22. [CrossRef]
15. Wei, C.; Dong, X.; Yu, D.; Zhang, T.; Zhao, W.; Ma, Y.M. Spatio-temporal variations of rainfall erosivity, correlation of climatic indices and influence on human activities in the Huaihe River Basin, China. *CATENA* **2022**, *217*, 106486. [CrossRef]

16. Matthews, F.; Panagos, P.; Verstraeten, G. Simulating event-scale rainfall erosivity across European climatic regions. *CATENA* **2022**, *213*, 106157. [CrossRef]
17. Diodato, N.; Borrelli, P.P.; Bellocchi, G. Global assessment of storm disaster-prone areas. *PLoS ONE* **2022**, *17*, e0272161. [CrossRef]
18. Ponjiger, T.M.; Lukić, T.; Basarin, B.; Jokic, M.; Wilby, R.L.; Pavić, D.; Mesaroš, M.; Valjarević, A.; Milanovic, M.; Morar, C. Detailed analysis of spatial–temporal variability of rainfall erosivity and erosivity density in the central and southern Pannonian basin. *Sustainability* **2021**, *13*, 13355. [CrossRef]
19. Zhang, J.P.; Ren, Y.L.; Jiao, P.; Xiao, P.Q.; Li, Z. Changes in rainfall erosivity from combined effects of multiple factors in China's Loess Plateau. *CATENA* **2022**, *216*, 106373. [CrossRef]
20. Bezak, N.; Mikoš, M.; Borrelli, P.; Liakos, L.; Panagos, P. An in-depth statistical analysis of the rainstorms erosivity in Europe. Catena. *CATENA* **2021**, *206*, 105577. [CrossRef]
21. Yang, Y.D.; Xu, Z.R.; Zheng, W.W.; Wang, S.H.; Kang, Y.B. Rain belt and flood peak: A study of the extreme precipitation event in the Yangtze river basin in 1849. *Water* **2021**, *13*, 2677. [CrossRef]
22. Jia, L.; Li, Z.B.; Li, P.; Zhang, J.Z.; Wang, A.N.; Ma, L.; Xu, G.C.; Zhang, X. Temporal and spatial variation of rainfall erosivity in the Loess Plateau of China and its impact on sediment load. *CATENA* **2022**, *210*, 105931. [CrossRef]
23. Wang, L.P.; Wang, X.R.; Wang, W.G. Research and application of comprehensive intensity evaluation method for regional rainfall process in China. *J. Nat. Disasters* **2015**, *24*, 186–194. [CrossRef]
24. Zou, Y.; Ye, D.X.; Lin, Y.; Liu, A.M. A quantitative method for assessment of regional rainstorm intensity. *J Appl. Meteor. Sci.* **2014**, *25*, 360–364.
25. Han, X.J.; Sum, X.W.; Li, S.; Wang, M.H.; Li, G.X.; Chen, Y.; Wang, G.C. Disaster-causing index of rainstorm and preassessment of disaster effect in Liaoning province. *J. Meteorol. Environ.* **2014**, *30*, 80–84. [CrossRef]
26. Chen, H. Projected change in extreme rainfall events in China by the end of the 21st century using CMIP5 models. *Chin. Sci. Bull.* **2013**, *58*, 1462–1472. [CrossRef]
27. Chen, H.; Sun, J. Increased population exposure to precipitation extremes in China under global warming scenarios. *Atmos. Ocean. Sci. Lett.* **2020**, *13*, 63–70. [CrossRef]
28. Patricola, C.M.; Wehner, M.F. Anthropogenic influences on majortropical cyclone events. *Nature* **2018**, *563*, 339–346. [CrossRef]
29. Wang, G.; Wang, D.; Trenberth, K.E.; Erfanian, A.; Yu, M.; Bosilovich, M.G.; Parr, D.T. The peak structure and future changes of the relationships between extreme precipitation and temperature. *Nat. Clim. Change* **2017**, *7*, 268–274. [CrossRef]
30. Scoccimarro, E.; Gualdi, S.; Bellucci, A.; Zampieri, M.; Navarra, A. Heavy precipitation events in a warmer climate: Results from CMIP5 models. *J. Clim.* **2013**, *26*, 7902–7911. [CrossRef]
31. Trenberth, K.E.; Fasullo, J.T.; Shepherd, T.G. Attribution of climate extreme events. *Nat. Clim. Change* **2015**, *5*, 725–730. [CrossRef]
32. Liu, Y.; Li, L.; Zhang, W.; Chan, P.; Liu, Y. Rapid identification of rainstorm disaster risks based on an artificial intelligence technology using the 2DPCA method. *Atmos. Res.* **2019**, *227*, 157–164. [CrossRef]
33. Gao, T.; Wang, H. Trends in precipitation extremes over theYellow River Basin in North China: Changing properties and causes. *Hydrol. Process.* **2017**, *31*, 2412–2428. [CrossRef]
34. Omer, A.; Elagib, N.A.; Zhuguo, M.; Saleem, F.; Mohammed, A. Water scarcity in the Yellow River Basin under future climate change and human activities. *Sci. Total Environ.* **2020**, *749*, 141446. [CrossRef] [PubMed]
35. Yuan, Z.; Yan, D.; Yang, Z.; Xu, J.; Huo, J.; Zhou, Y.; Zhang, C. Attribution assessment and projection of natural runoff change in theYellow River Basin of China. *Mitig. Adapt. Strateg. Glob. Change* **2016**, *23*, 27–49. [CrossRef]
36. Li, C.; Jian, T.; Wang, Y.J.; Miao, L.J.; Li, S.Y.; Chen, Z.Y.; Lü, Y.R. Simulation and estimation of future air temperature in upper basin of the Yellow River based on CMIP6 models. *J. Glaciol. Geocryol.* **2022**, *44*, 171–178. [CrossRef]
37. Chen, H.P.; Sun, J.Q.; Lin, W.Q.; Xu, H.W. Comparison of CMIP6 and CMIP5 models in simulating climate extremes. *Sci. Bull.* **2020**, *65*, 1415–1418. [CrossRef]
38. Zhai, J.; Mondal, S.K.; Fischer, T.; Wang, Y.; Su, B.; Huang, J.; Tao, H.; Wang, G.; Ullah, W.; Uddin, J. Future drought characteristics through a multi-model ensemble from CMIP6 over South Asia. *Atmos. Res.* **2020**, *246*, 105111. [CrossRef]
39. Sui, X.; Qi, Y. Dynamic assessment of ecological carrying capacity of Yellow River Basin in Qinghai province. *Chin. J. Ecol.* **2007**, *26*, 406–412.
40. Taylor, K.E.; Stouffer, R.J.; Meehl, G.A. An overview of CMIP5 and the experiment design. *Bull. Am. Meteorol. Soc.* **2012**, *93*, 485–498. [CrossRef]
41. Sillmann, J.; Kharin, V.; Zwiers, F.W.; Zhang, X.; Bronaugh, D. Climate extremes indices in the CMIP5 multimodel ensemble: Part 2. future climate projections. *JGR Atmos.* **2013**, *118*, 2473–2493. [CrossRef]
42. Kharin, V.V.; Zwiers, F.W.; Zhang, X.; Wehner, M. Changes in temperature and precipitation extremes in the CMIP5 ensemble. *Clim. Change* **2013**, *119*, 345–357. [CrossRef]
43. O'Neill, B.C.; Kriegler, E.; Ebi, K.L.; Benedict, E.K.; Riahi, K.; Rothman, D.S.; van Ruijven, B.J.; van Vuuren, D.P.; Birkmann, J.; Kok, K.; et al. The roads ahead: Narratives for shared socioeconomic pathways describing world futures in the 21st century. *Glob. Environ. Change* **2017**, *42*, 169–180. [CrossRef]
44. Gao, J. *Global 1-km Downscaled Population Base Year and Projection Grids Based on the Shared Socioeconomic Pathways*; NASA Socioeconomic Data and Applications Center (SEDAC): Palisades, NY, USA, 2020. [CrossRef]
45. Administration for Market Regulation of Qinghai Province. *Classification Index of Meteorological Disasters (DB63/T372-2018)*; Administration for Market Regulation of Qinghai Province: Xining, China, 2018; p. 9.

46. Zhou, B.T.; Yu, L. Managing climate disaster risks and promoting climate change adaptation. *Disaster Reduct. China* **2012**, *174*, 18–19.
47. Rupp, D.E.; Abatzoglou, J.T.; Hegewisch, K.C.; Mote, P.W. Evaluation of CMIP5 20th century climate simulations for the Pacific Northwest USA. *Geophys. Res. Atmos.* **2013**, *118*, 10884–10906. [CrossRef]
48. Delgado, A.; Romero, I. Environmental conflict analysis using an integrated grey clustering and entropy-weight method: A case study of a mining project in Peru. *Environ. Model. Softw.* **2016**, *77*, 108–121. [CrossRef]
49. Wei, F.Y. *Modern Techniques of Statistical Diagnosis and Prediction of Climate*, 2nd ed.; Meteorological Press: Beijing, China, 2007.
50. Yue, S.; Pilon, P.; Phinney, B.; Cavadias, G. The influence of autocorrelation on the ability to detect trends in hydrological series. *Hydrol. Process.* **2002**, *16*, 1807–1829. [CrossRef]
51. Sun, S.; Dai, T.L.; Wang, Z.Y.; Ming, C.J.; Chao, Q.C.; Shi, P.J. Projected increases in population exposure of daily climate extremes in eastern China by 2050. *Adv. Clim. Change Res.* **2021**, *12*, 804–813. [CrossRef]
52. Su, X.; Shao, W.W.; Liu, J.H.; Jiang, Y.Z.; Wang, K.B. Dynamic Assessment of the Impact of Flood Disaster on Economy and Population under Extreme Rainstorm Events. *Remote Sens.* **2021**, *13*, 3924. [CrossRef]